Published in final edited form as:
Invest Ophthalmol Vis Sci. 2007 July ; 48(7): 2967–2974.

Modeling the Behavior of Uveal Melanoma in the Liver

Robert Folberg[1], **Lu Leach**[1], **Klara Valyi-Nagy**[1], **Amy Y. Lin**[1], **Marsha A. Apushkin**[1], **Zhuming Ai**[2], **Vivian Barak**[3], **Dibyen Majumdar**[4], **Jacob Pe'er**[5], and **Andrew J. Maniotis**[1]

1*From the Department of Pathology, University of Illinois at Chicago, Chicago, Illinois*

2*From the Virtual Reality in Medicine Laboratory, Department of Biomedical and Health Information Sciences, University of Illinois at Chicago, Chicago, Illinois*

4*From the Department of Mathematics, Statistics, and Computer Science, University of Illinois at Chicago, Chicago, Illinois*

3*From the Immunology Laboratory for Tumor Diagnosis, Hadassah-Hebrew University Medical Center, Jerusalem, Israel.*

5*From the Department of Ophthalmology, Hadassah-Hebrew University Medical Center, Jerusalem, Israel.*

Abstract

Purpose—To model the behavior of uveal melanoma in the liver.

Methods—A 15-μL suspension of metastatic MUM2B or either primary OCM1 or M619 uveal melanoma cells was injected into the liver parenchyma of 105 CB17 SCID mice through a 1-cm abdominal incision. Animals were killed at 2, 4, 6, or 8 weeks after injection. Before euthanatization, 3% FITC-BSA buffer was injected into the retro-orbital plexus of one eye of three mice. Liver tissues were examined by light and fluorescence microscopy, and were stained with human anti-laminin. Vasculogenic mimicry patterns were reconstructed from serial laser scanning confocal microscopic stacks.

Results—OCM1a cells formed microscopic nodules in the mouse liver within 2 weeks after injection and metastasized to the lung 6 weeks later. By contrast, M619 and MUM2B cells formed expansile nodules in the liver within 2 weeks and gave rise to pulmonary metastases within 4 weeks after injection. Vasculogenic mimicry patterns, composed of human laminin and identical with those in human primary and metastatic uveal melanomas, were detected in the animal model. The detection of human rather than mouse laminin in the vasculogenic mimicry patterns in this model demonstrates that these patterns were of tumor cell origin and were not co-opted from the mouse liver microenvironment.

Conclusions—There are currently no effective treatments for metastatic uveal melanoma. This direct-injection model focuses on critical interactions between the tumor cell and the liver. It provides for translationally relevant approaches to the development of new modalities to detect small tumor burdens in patients, to study the biology of clinical dormancy of metastatic disease in uveal melanoma, to design and test novel treatments to prevent the emergence of clinically manifest liver metastases after dormancy, and to treat established uveal melanoma metastases.

The clinical tendency for uveal melanoma to spread first and preferentially to the liver is well documented.[1] In developing animal models of uveal melanoma, most investigators have focused on studying the mechanisms by which tumors develop in the animal eye and generate

Corresponding author: Robert Folberg, Department of Pathology, University of Illinois at Chicago, 840 S. Wood Street, 110 CSN (MC847), Chicago, IL 60612; rfolberg@uic.edu.

Disclosure: **R. Folberg**, None; **L. Leach**, None; **K. Valyi-Nagy**, None; **A.Y. Lin**, None; **M.A. Apushkin**, None; **Z. Ai**, None; **V. Barak**, None; **D. Majumdar**, None; **J. Pe'er**, None; **A.J. Maniotis**, None

hepatic metastases. Strategies for modeling primary uveal melanoma include the induction of tumors by feline retroviruses[2] and chemical carcinogens,[3,4] the development of transgenic models of primary uveal melanoma,[5-10] and the transplantation of melanoma cell lines—animal[11-15] and human[16-18]—to the animal eye. The literature summarizing animal models of uveal melanoma was reviewed recently.[19]

Models of uveal melanoma based on the implantation of tumor into the animal eye have been the focus of several innovative experimental approaches designed to reduce the spread of tumor from the eye to the liver.[16,20-23] In these models, the entire metastatic cascade—dislodgement from the primary tumor, entrance to the microcirculation, extravasation, and proliferation within the liver—are all potential targets of experimental therapy. Certainly, the prevention of metastasis in high-risk patients is a clinical priority; however, after a patient develops metastatic uveal melanoma, the clinical focus shifts entirely to eradication of the established metastases. Although there has been considerable progress in developing vision-sparing alternatives to the removal of the eye for treatment of the primary tumor, there have been no significant improvements in the treatment of hepatic metastases.

Little is known in the ophthalmic research community about the biological behavior of uveal melanoma once it has arrived in the liver. Since ophthalmic oncologic research has focused to date nearly exclusively on the entire metastatic cascade by introducing uveal melanoma into the eye of experimental animals, we modified a colon cancer model of direct injection[24] to study the biology of uveal melanoma in the liver. We discovered that nodules of uveal melanoma develop in predictable time courses in the mouse liver, followed by secondary melanoma deposits in the lungs. Hepatic tumor nodules and secondary pulmonary lesions develop within 4 to 8 weeks after injection into the liver, depending on the invasive properties of the cell line injected. The histology of melanoma nodules in the liver that form after direct injection in mice is similar to the histology of human metastatic uveal melanoma in the liver. Similar to primary and metastatic human uveal melanomas, laminin-rich vasculogenic mimicry patterns formed in hepatic lesions, and these patterns conducted fluid. The direct-injection model can therefore be used to study biological events that are involved in establishing and maintaining foci of uveal melanoma in the liver, and this model provides an additional approach to the development of novel, effective, and nontoxic therapies targeted to the treatment of metastatic uveal melanoma.

Materials and Methods

Cell Lines

Cell lines were derived from primary and metastatic uveal melanomas (M619 and MUM2B), as described previously.[25] Human WI38 fibroblasts were obtained from ATTC (Manassas, VA). The OCM1a cell line was a generous gift of June Kan-Mitchell (Karmanos Cancer Institute, Wayne State University, Detroit, MI). All cell lines have been authenticated as human[26] and as free of mycoplasma and common viral pathogens. These cell lines have been shown repeatedly to model the behavior of primary and metastatic uveal melanoma in vivo.[25,27] The primary uveal OCM1a melanoma cell line is poorly invasive in membrane-invasion culture system[28] assays and does not form vasculogenic mimicry patterns in three-dimensional (3D) cultures. By contrast, the M619 primary uveal melanoma cell line and the metastatic MUM2B uveal melanoma cell lines are highly invasive in MICS assays and form vasculogenic mimicry patterns in 3D cultures.[25] From each cell line, 5 million cells were grown in 1% agar–coated, 60-mm tissue culture dishes containing 15% heat-inactivated fetal bovine serum, glutamine, and MEM/EBSS (minimum essential medium with Earle's balanced salts solution; Hyclone, Logan, UT) until spheroids formed (typically within 2 days). WI38 fibroblasts were prepared for injection by using the same protocol but substituting DMEM (BioWhitaker,

Walkersville, MD) for MEM/EBSS and 10% fetal bovine serum. When the spheroids reached the size of 200 to 500 μm, they were injected directly into the liver of SCID mice.

Implantation Technique

Each mouse was anesthetized before surgery with ketamine (100 mg/kg) and xylazine (5 mg/kg) via intraperitoneal injection. A small horizontal abdominal incision (1 cm) was made in the left upper quadrant so that the left lobe of the liver was exposed. Spheroids of melanoma cells from one of the three lines were drawn into a Hamilton syringe with a 29-gauge needle creating a 15 μL slurry that was injected into the parenchyma of the exposed liver with the assistance of a stereomicroscope (American Optical Company, Buffalo, NY), roughly after a protocol described previously to establish models of colon cancer in the liver.[24] It had been shown previously that the use of cell slurries fashioned from tumor cell spheroids was particularly effective in establishing animal models of primary uveal melanoma in the rat.[29] Gentle pressure was applied to the hepatic injection site for 1 minute with a cotton-tipped applicator. After tumor cell injection, the left lobe of the liver was repositioned into the peritoneal cavity, and the abdominal wall was then closed with a 6-0 absorbable suture (Ethicon, Somerville, NJ).

Time-Course Experiments

Preliminary experiments indicated that 4 weeks after intrahepatic injection of tumor cells, mice receiving M619 or MUM2B cells approached a 20% loss in body weight, whereas mice receiving OCM1a cells appeared healthy at the same time point. Ninety additional male SCID CB-17 mice (Harlan Sprague-Dawley, Indianapolis, IN), 19 to 21 g, were divided into six experimental groups of 15 animals each. The liver of each animal received one of the three cell lines, and for each cell line, animals were euthanatized at either 2 or 4 weeks after implantation (a total of six groups of animals, 15 animals per group). The liver of each of 15 additional animals was injected with OCM1a cells and observed for 7 (2 animals) or 8 (13 animals) weeks. WI38 fibroblasts were injected in the liver of five mice and these animals were euthanatized 4 weeks later. A complete necropsy was performed on each animal. The identification of metastases was made from the examination of histologic preparations of the bread-loafed liver and other viscera stained with hematoxylin-eosin rather than by gross examination. One hematoxylin-eosin–stained section of each organ was scanned by one of the investigators (RF) for the presence or absence of metastases. On the average, five slides from each animal were reviewed. Typically, three of these slides represented bread-loaf sections through the liver and lungs. The size of hepatic uveal melanoma tumor nodules in the liver was measured directly from glass slides.[30] Differences in the size of lesions for each cell line were compared at different time points, and differences in the sizes of lesions between time points were studied with the Kruskal-Wallis test. All animal protocols were approved by the Animal Care Committee of the University of Illinois at Chicago and conformed to the ARVO Statement for the Use of Animals in Ophthalmic and Vision Research.

Perfusion Studies

Before euthanatization, three mice in which OCM1a cells had been injected 6 weeks earlier were perfused with fluorescent bovine serum albumin (BSA; Sigma-Aldrich, St. Louis, MO). Each animal was injected with the ketamine-xylazine cocktail for the implantation followed by the injection of 0.2 mL of 3% FITC-BSA into the retrobulbar orbital plexus of one eye. After 45 minutes of observation, animals were euthanatized. Liver tissue with tumor nodules was snap frozen, sectioned on a cryostat at 4 μm, and viewed with a microscope equipped for fluorescence (BX40; Olympus America, Melville, NY). Digital images were then captured (Optronics MagnaFire Camera; Optronics, Goletta, CA).

Immunohistochemistry

The histologic demonstration of vasculogenic mimicry patterns in primary uveal melanomas is associated with the development of metastatic melanoma,[31] and these patterns have been described in liver and extrahepatic uveal melanoma metastases.[32] Because these patterns have been confused with fibrovascular septa when uveal melanoma cells were implanted subcutaneously in mice,[33] the patterns were stained with laminin rather than the more nonspecific periodic acid-Schiff (PAS), used originally to demonstrate vasculogenic mimicry patterns in tissue sections.[34]

Unstained slides cut at 4 μm from all melanoma nodules in the liver and pulmonary metastases (as identified on hematoxylin-eosin stained sections) were stained with either a mouse monoclonal antibody (L8271, clone LAM 89; Sigma-Aldrich, St. Louis, MO) specific for human laminin or a rabbit polyclonal anti-laminin antibody (Z0097; Dako, Carpinteria, CA) that cross-reacts with both mouse and human laminin (both in a dilution of 1:200). Formalin fixed, paraffin-embedded tissue samples were sectioned at 4-μm thickness and mounted on slides (Superfrost/Plus; Erie Scientific Company, Portsmouth, NH). The slides were deparaffinized in xylene, rehydrated through a decreasing ethanol gradient, and rinsed in distilled water followed by antigen unmasking with a 10× concentrated retrieval solution (Target Retrieval Solution; Dako), according to the manufacturer's instructions. They were then rinsed in phosphate-buffered saline (PBS) for 5 minutes. The tissue sections were exposed to a blocking solution (Peroxidase Blocking Reagent; Dako) for 10 minutes at room temperature. The slides were pretreated with proteinase K (Dako) for 5 minutes and then with protein-blocking solution (Protein Block Serum-Free; Dako) for 10 minutes at room temperature. They were rinsed and incubated with one of the two anti-laminin antibodies for 30 minutes at room temperature, rinsed, and treated with a labeled polymer (EnVision Plus; Dako) for 30 minutes at room temperature. Laminin staining was detected by 3,3′-diaminobenzidine (DAB Plus; Dako) for 10 minutes. (Each of the three cell lines generates amelanotic tumors when implanted into animal hosts.) The slides were rinsed in distilled water, counterstained, and dehydrated through an alcohol gradient and mounted (Permount; Biomeda, Foster City, CA).

For the demonstration of mouse endothelial cells in frozen sections of the mouse liver, the following protocol was used. Frozen sections were cut at 4 μm and were fixed in acetone. Slides were placed in PBS for 15 minutes. An H_2O_2 block was applied at room temperature for 10 minutes, and the slides were rinsed with PBS followed by the protein blocking solution, as described earlier, for 10 minutes. The slides were blotted and exposed to anti-mouse CD31 (PECAM-1; BD-Pharmingen, San Diego, CA), 1:20 dilution at room temperature for 60 minutes. Chromogen detection and slide preparation followed the protocol described earlier.

Digital photomicrographs were obtained (with either a MagnaFire Camera; Optronics mounted on a BX40 microscope; Olympus America, or with a CS Digital Scanner; Aperio Technologies, Vista, CA).

3D Reconstruction of Vasculogenic Mimicry Patterns in Melanoma Hepatic Deposits in the Mouse

Vasculogenic mimicry patterns in human uveal melanoma tissue, both primary and metastatic, have been reconstructed with high fidelity from serial paraffin-embedded sections by methods described in detail previously.[35-37]

Briefly, 14 serial paraffin-embedded sections cut at 4 μm were dual-labeled with antibodies to human laminin and to S-100 protein. We have shown that human uveal melanoma tends to stain diffusely with antibodies to S-100 proteins, whereas the distribution of other melanocytic

markers is patchy.[38] After the sections were treated as described earlier through the steps of blocking solution and proteinase K, the slides were incubated with monoclonal mouse anti-laminin antibody (L8271, clone LAM 89; Sigma-Aldrich) at a titer of 1:200 for 30 minutes at room temperature. The slides were rinsed then treated with protein block (Protein Block Serum-Free; Dako) for 10 minutes, blotted, and then treated with Alexa Fluor 488 mouse-goat antibody (Invitrogen-Molecular Probes, Eugene, OR) at a 1:400 dilution for 30 minutes at room temperature. They were blocked with protein block as described earlier and incubated with S100 rabbit antibody (Z0311; Dako) at a dilution of 1:200 for 30 minutes at room temperature, rinsed, blocked with protein block for 10 minutes, blotted, and exposed to Alexa Fluor 594 rabbit-goat antibody (Invitrogen-Molecular Probes) at a titer of 1:400 for 30 minutes at room temperature. They were then rinsed in distilled water and mounted (Faramount; Dako) and kept in a dark place until screened.

To locate areas of vasculogenic mimicry patterns, we first studied the slides by routine immunofluorescence microscopy (BX40; Olympus). Fields for reconstruction were captured with the digital camera (MagnaFire; Optronics) for each chromogen, and the images were merged (MagnaFire software; Optronics). Each of the 14 serial sections was then examined with a laser scanning confocal microscope (LSM 510; Carl Zeiss Meditech, Thornwood, NY) with a 40× objective. Images were stored in laser scanning microscope format and converted on computer (LSM Image Browser software, ver. 2.50.0929; Carl Zeiss Meditec, Jena, Germany) into tagged image file format (TIFF). The 3D reconstruction was accomplished by using an immersive virtual reality environment (Immersadesk; Fakespace, Kitcherner, Ontario, Canada), as described in detail previously.[35-37]

Results

The Establishment of Uveal Melanoma Deposits in the Mouse Liver and Secondary Metastases

MUM2B cells, which are highly invasive in vitro and which were developed from a human liver uveal melanoma metastasis, formed tumor nodules in the mouse liver within 2 weeks after implantation in 9 (60%) of the 15 animals injected. The MUM2B cells not only formed expansile nodules within the liver, but spread as a plaque over the liver surface. In four of the nine animals in which liver nodules developed at 2 weeks after implantation, tumor had spread by direct extension to the abdominal viscera, but secondary metastases to the lung were not identified. However, by 4 weeks after injections, tumor had spread locally to the abdominal viscera in 14 (93%) animals and to the lungs in 8 (53%). Metastases to hilar lymph nodes were identified in one animal, and tumor emboli within blood vessels were identified in a different animal.

M619 cells, which are also highly invasive in vitro and which were developed from a primary uveal melanoma, formed tumor nodules in the liver in 10 (67%) of the 15 animals in this group at 2 weeks after injection, without evidence of local invasion along the surface of the liver and into the abdomen. At 4 weeks after injection, all 15 mouse livers contained nodules of melanoma. In 8 of these animals, tumor was confined to the liver, but in 7 animals, tumor not only expanded within the liver but also grew as a surface plaque over the liver. Adjacent abdominal visceral organs were infiltrated by tumor in 11 animals. Metastases were identified in hilar lymph nodes in three animals, and pulmonary metastases were identified in one.

OCM1a cells, which are poorly invasive in vitro, established microscopic liver nodules in 8 (53%) of the 15 animals within 2 weeks. Nodules formed by OCM1a were expansile, remaining within the liver parenchyma and, unlike MUM2B and M619 cells, growth along the surface of the liver was never observed, nor was there any evidence of local spread to the abdominal viscera at this time point. At 4 weeks after injection, tumor nodules were present in nine animals

without evidence of surface plaque, abdominal spread, or pulmonary metastases. At 6 weeks after injection, tumor nodules were observed in each of the six animals observed to this time point with focal spread into the abdomen in five animals and no evidence of pulmonary metastases. In each of the nine animals observed for more than 6 weeks, tumor nodules developed in the liver and in seven (78%), abdominal spread was identified. Pulmonary metastases were identified in one of the two animals observed until 7 weeks and in five of the six animals observed for 8 weeks after injection.

Four weeks after injection of WI38 fibroblasts into the mouse liver, no lesions were detected.

Animals receiving M619 and MUM2B cells were not observed beyond 4 weeks, to minimize distress to the animals because of the high incidence of secondary metastases by that time point. Representative histologic findings are presented in Figure 1 and the time-course for tumor development after implantation for each of the three cell lines is summarized in Table 1. As expected, there were significant increases in the size of uveal melanoma tumors in the mouse liver over time for each of the three cell lines, as summarized in Table 2.

Demonstration of Vasculogenic Mimicry in Hepatic Nodules

Highly invasive M619 and MUM2B cells stained intensely and uniformly positive for laminin at all time points. Although laminin-positive loops, identical with laminin-positive vasculogenic mimicry patterns in human metastases in the liver,[32,39] were identified in some tumor nodules formed by M619 and MUM2B cells in the liver, the intensity of laminin staining obscured the discrimination of intralesional patterning. By contrast, OCM1a cells were diffusely but very weakly laminin-positive in all lesions and intensely staining laminin-positive loops and networks of back-to-back loops were consistently and easily identified in lesions formed in the liver as early as 2 weeks after injection (0.4 mm in diameter). Laminin-positive vasculogenic mimicry patterns, identical with those seen in human tumors, were identified in larger intrahepatic nodules formed by OCM1a at 6 to 8 weeks (Fig. 2A) and within very small secondary metastases to the lung formed by MUM2B cells 4 weeks after implantation (Fig. 2B). Vasculogenic mimicry patterns were formed more consistently by OCM1a cells in the context of the liver than by M619 or MUM2B cells.

Vasculogenic mimicry patterns were visualized in tissues labeled by the polyclonal anti-laminin antibody that recognizes both mouse and human laminin. The monoclonal anti-laminin antibody, specific for human laminin, did not label mouse control tissues, such as renal tubules or glomeruli, nor did the antibody label internal controls such as vessels in the mouse liver, but looping vasculogenic mimicry patterns were clearly evident in the OCM1a tumor nodules in the liver (Figs. 2C-F).

Three-dimensional reconstructions of vasculogenic mimicry patterns in OCM1a-generated liver nodules revealed the laminin-positive patterns to represent thin envelopes wrapped around branching cylinders of OCM1a tumor cells (Fig. 3). The 3D characteristics of these patterns can be better appreciated by viewing Movie 1, available online at http://www.iovs.org/cgi/content/full/48/7/2967/DC1. Reconstructions of OCM1a-generated tumor nodules in the mouse liver were identical topologically to reconstructions of human primary[35] and metastatic uveal melanomas[40] reported previously.

Because vasculogenic mimicry patterns were most highly developed in animals whose livers were injected with OCM1a cells between 6 and 8 weeks, three of these animals were perfused by FITC-BSA before euthanatization. In contrast to the radial distribution of the tracer in hepatic sinusoids adjacent to central venules in the uninvolved hepatic parenchyma (Fig. 4A), tracer within the tumor nodule was distributed as back-to-back loops (Fig. 4B). It is known

that endothelial cell-lined blood vessels do not appear as back-to-back loops on thin, 2D histologic sections.[41]

Discussion

The model of metastatic uveal melanoma generated by the direct intrahepatic injection of human uveal melanoma cells faithfully reproduces the histology of metastatic uveal melanoma to the liver and is not associated with ocular morbidity. Looping vasculogenic mimicry patterns are generated in both the liver nodules and the secondary metastases (Fig. 1). The 3D architecture of these patterns in the model (Fig. 3) is identical with the architecture of these patterns in human primary[35] and metastatic uveal melanoma,[40] and these patterns appear to constitute a perfusion pathway (Fig. 4) in the model as they do in other animal models of vasculogenic mimicry[33] and in human tumors.[31] Depending on the invasive behavior of the cell line used, the model may not simulate the disease in patients with endstage metastatic uveal melanoma. For example, some of the most invasive uveal melanoma cell lines used in this study (M619 and MUM2B) not only generated hepatic nodules and secondary metastases to the lungs, but also eventually spread throughout the abdomen, a behavior sometimes seen in patients but not typical of the clinical course of metastatic uveal melanoma. However, the implantation of OCM1a cells into the mouse liver closely simulated the clinical behavior of human uveal melanoma hepatic metastases.

Metastatic disease is seldom identified in patients with primary uveal melanoma at the time of the initial diagnosis and treatment.[42] Regardless of the modality used to eradicate the primary tumor, metastases do not typically become clinically manifest in patients until years, sometimes many years, later.[43] It is therefore likely that tumor has already spread to the liver at the time of the initial diagnosis and treatment. Although the direct injection of human uveal melanoma cells into the SCID mouse liver does not model the complete natural history of the metastatic cascade from the eye to the target organ, the direct-injection model focuses on critical interactions between the tumor cell and the liver. Considering the disappointing reality that no significant progress has been made to date in the treatment of patients with metastatic uveal melanoma, the direct-injection model provides for translationally relevant approaches to: (1) the development of new modalities to detect small tumor burdens in patients, (2) the biology of clinical dormancy of metastatic disease in uveal melanoma, (3) the design and testing of novel treatments to prevent the emergence of clinically manifest liver metastases after dormancy, and (4) the treatment of established metastatic uveal melanoma.

By using the direct-injection model and focusing on the interaction between the uveal melanoma cell and the liver, we were able to resolve unequivocally an ongoing controversy among uveal melanoma researchers—the histogenesis of vasculogenic mimicry patterns. Although uveal melanoma cells generate vasculogenic mimicry patterns in vitro without the participation of endothelial cells or fibroblasts,[25] some investigators have proposed that these patterns represent “fibrovascular septa”[44] originating as a stromal response generated by the host.[45] Although it has been shown recently that uveal melanoma cells are capable of generating extracellular matrix proteins that have been identified in vasculogenic mimicry patterns,[34] it remained theoretically possible that the patterns were composed of proteins co-opted from the microenvironment. By exploiting significant differences between human and mouse laminin[46] and using an antibody specific for human laminin, it was possible to demonstrate that laminin in vasculogenic mimicry patterns in the human uveal melanoma nodules is of human origin and thus originates from the tumor instead of the mouse host (Fig. 2).

The direct-injection model may be especially useful in developing new strategies for the early detection of small tumor burdens in the liver. For many years, oncologists have monitored liver

enzymes on sequential visits after the treatment of the primary tumor to detect metastatic uveal melanoma. However, the sensitivity and specificity of liver enzymes in detecting metastasis is disappointingly low,[47] and patients may present with significant hepatic replacement by tumor and normal liver enzymes.[48] The sensitivity of hepatic ultrasound in detecting metastases from uveal melanoma is high, but the specificity is low.[49] One clinical investigation team concluded that ultrasound screening did not contribute to an improvement in outcome and called for the development of "better screening tests and more effective multimodality treatments… to improve survival in uveal melanoma patients with hepatic metastases."[50]

After implantation into the mouse liver, human uveal melanoma cells formed very small tumor nodules of melanoma at predictable times (Table 2). Therefore, it is possible to screen mouse serum in the direct-injection model to identify human-secreted proteins that may be very sensitive in detecting extremely small tumor burdens in vivo. A large number of putative biomarkers are now being identified through genomic or proteomic analyses of uveal melanoma cells and tissues. Screening putative biomarkers on banked human sera is wasteful of sera and is expensive.

The biological mechanisms underlying the latent emergence of clinical metastases in patients with uveal melanoma can also be explored in the direct-injection model. Certainly, the direct injection of uveal melanoma cells into SCID mice compromises the ability to study T-cell–dependent immune responses to the tumor, a limitation also found in most natural history models in immunosuppressed animals. However, investigators may vary several experimental conditions to model tumor dormancy independent of immune regulation of the tumor. For example, in the direct-injection model, it takes nearly 6 to 8 weeks for OCM1a cells to form tumor nodules in the liver of comparable size to nodules produced by M619 and MUM2B cells in only 4 weeks, pointing to intrinsic properties of the tumor cell as one possible explanation for dormancy. Investigators may use a variety of different cell lines to further model dormancy as an intrinsic property of the tumor cell.

Furthermore, with regard to the phenomenon of dormancy in uveal melanoma in the liver, it is becoming apparent that the behavior of tumor cells is contextual and can be profoundly influenced by the tumor's microenvironment. For example, Kulesa et al.[51] have shown recently that highly invasive cutaneous melanoma cells injected into the embryonic chick do not form tumors but rather are reprogrammed to populate benign neural crest– derived structures. Thus, although OCM1a uveal melanoma cells did not generate vasculogenic mimicry patterns in 3D culture conditions, these cells do generate these patterns when placed into the liver (Fig. 2A). It is interesting that although all three cell lines used in this study generated some degree of vasculogenic mimicry patterning in the liver, these patterns were most prominent and were found most consistently in nodules formed by OCM1a cells. The recently reported finding associating the generation of vasculogenic mimicry patterning by uveal melanoma cells with dampening of the metastatic phenotype (suppression of proliferation, decreased migration and invasion, and even phenotypic reversion to a spindle A morphology)[52] may therefore provide yet another partial explanation for the relative "latency" of OCM1a cells in generating large nodules in the liver and secondary metastases compared with M619 and MUM2B cells.

The direct-injection model may be especially useful in developing chemoprevention strategies to abort the emergence of clinically relevant metastases from micrometastases in patients with primary uveal melanoma who are at high risk for metastasis. Finally, the direct-injection model may be useful in designing treatments for patients with more advanced hepatic metastases.

Thus, by focusing on the interaction of uveal melanoma cells and the liver, the direct-injection model facilitates a large number of clinically relevant experiments. The direct-injection model

therefore complements established natural history models that span the panorama of the metastatic cascade.

Acknowledgements

Supported by Grants R01 EY10457 (RF) and Core Grant EY 10797 (Department of Ophthalmology and Visual Sciences) from the National Eye Institute, Bethesda, MD.

References

1. McLean IW. The biology of haematogenous metastasis in human uveal malignant melanoma. Virchows Arch A Pathol Anat 1993;422:433–437.
2. Albert DM, Shadduck JA, Craft JL, Niederkorn JY. Feline uveal melanoma model induced with feline sarcoma virus. Invest Ophthalmol Vis Sci 1981;20:606–624. [PubMed: 6260703]
3. Folberg R, Baron J, Reeves RD, Stevens RH, Tse DT. Primary melanocytic lesions of the rabbit choroid following topical application of 7,12-dimethylbenzanthracene: preliminary observations. J Toxicol Cutan Ocul Toxicol 1990;9:313–334.
4. Pe'er J, Folberg R, Massicotte SJ, et al. Clinicopathologic spectrum of primary uveal melanocytic lesions in an animal model. Ophthalmology 1992;99:977–986. [PubMed: 1630787]
5. Bradl M, Klein-Szanto A, Porter S, Mintz B. Malignant melanoma in transgenic mice. Proc Natl Acad Sci USA 1991;88:164–168. [PubMed: 1846036]
6. Anand R, Ma D, Alizadeh H, et al. Characterization of intraocular tumors arising in transgenic mice. Invest Ophthalmol Vis Sci 1994;35:3533–3539. [PubMed: 8056529]
7. Syed NA, Windle JJ, Darjatmoko SR, et al. Transgenic mice with pigmented intraocular tumors: tissue of origin and treatment. Invest Ophthalmol Vis Sci 1998;39:2800–2805. [PubMed: 9856795]
8. Powell MB, Hyman P, Bell OD, et al. Hyperpigmentation and melanocytic hyperplasia in transgenic mice expressing the human T24 Ha-ras gene regulated by a mouse tyrosinase promoter. Mol Carcinog 1995;12:82–90. [PubMed: 7662120]
9. Kramer TR, Powell MB, Wilson MM, Salvatore J, Grossniklaus HE. Pigmented uveal tumours in a transgenic mouse model. Br J Ophthalmol 1998;82:953–960. [PubMed: 9828784]
10. Tolleson WH, Doss JC, Latendresse J, et al. Spontaneous uveal amelanotic melanoma in transgenic Tyr-RAS+ Ink4a/Arf−/− mice. Arch Ophthalmol 2005;123:1088–1094. [PubMed: 16087843]
11. Burns RP, Fraunfelder FT. Experimental intraocular malignant melanoma in the Syrian golden hamster. Am J Ophthalmol 1961;51:977–983. [PubMed: 13689204]
12. Niederkorn JY. T cell subsets involved in the rejection of metastases arising from intraocular melanomas in mice. Invest Ophthalmol Vis Sci 1987;28:1397–1403. [PubMed: 3497133]
13. Niederkorn JY, Sanborn GE, Gamel JW. Suicide enzyme inhibition as a chemotherapeutic strategy for controlling metastases derived from intraocular melanomas. Invest Ophthalmol Vis Sci 1987;28:1844–1850. [PubMed: 3117718]
14. Diaz CE, Rusciano D, Dithmar S, Grossniklaus HE. B16LS9 melanoma cells spread to the liver from the murine ocular posterior compartment (PC). Curr Eye Res 1999;18:125–129. [PubMed: 10223656]
15. Dithmar S, Rusciano D, Grossniklaus HE. A new technique for implantation of tissue culture melanoma cells in a murine model of metastatic ocular melanoma. Melanoma Res 2000;10:2–8. [PubMed: 10711634]
16. Apte RS, Niederkorn JY, Mayhew E, Alizadeh H. Angiostatin produced by certain primary uveal melanoma cell lines impedes the development of liver metastases. Arch Ophthalmol 2001;119:1805–1809. [PubMed: 11735791]
17. Mueller AJ, Maniotis AJ, Freeman WR, et al. An orthotopic model for human uveal melanoma in SCID mice. Microvas Res 2002;64:207–213.
18. Braun RD, Abbas A. Orthotopic human choroidal melanoma xenografts in nude rats with aggressive and nonaggressive PAS staining patterns. Invest Ophthalmol Vis Sci 2006;47:7–16. [PubMed: 16384938]

19. Grossniklaus HE, Dithmar S, Albert DM. Animal models of uveal melanoma. Mel Res 2000;10:195–211.
20. Ma D, Gerard RD, Li XY, Alizadeh H, Niederkorn JY. Inhibition of metastasis of intraocular melanomas by adenovirus-mediated gene transfer of plasminogen activator inhibitor type I (PAI-1) in an athymic mouse model. Blood 1997;90:2738–2746. [PubMed: 9326241]
21. Yang H, Dithmar S, Grossniklaus HE. Interferon alpha 2b decreases hepatic micrometastasis in a murine model of ocular melanoma by activation of intrinsic hepatic natural killer cells. Invest Ophthalmol Vis Sci 2004;45:2056–2064. [PubMed: 15223777]
22. Yang H, Akor C, Dithmar S, Grossniklaus HE. Low dose adjuvant angiostatin decreases hepatic micrometastasis in murine ocular melanoma model. Mol Vis 2004;10:987–995. [PubMed: 15623988]
23. Yang H, Grossniklaus HE. Combined immunologic and anti-angiogenic therapy reduces hepatic micrometastases in a murine ocular melanoma model. Curr Eye Res 2006;31:557–562. [PubMed: 16769615]
24. Kollmar O, Schilling MK, Menger MD. Experimental liver metastasis: Standards for local cell implantation to study isolated tumor growth in mice. Clin Exp Met 2004;21:453–460.
25. Maniotis AJ, Folberg R, Hess A, et al. Vascular channel formation by human melanoma cells in vivo and in vitro: vasculogenic mimicry. Am J Pathol 1999;155:739–752. [PubMed: 10487832]
26. Maniotis AJ, Valyi-Nagy K, Karavitis J, et al. Chromatin sensitivity to Alu I endonuclease is regulated by extracellular matrix and the cytoskeleton. Am J Pathol 2005;166:1187–1203. [PubMed: 15793298]
27. Maniotis AJ, Chen X, Garcia C, et al. Control of melanoma morphogenesis, endothelial survival, and perfusion by extracellular matrix. Lab Invest 2002;82:1031–1043. [PubMed: 12177242]
28. Welch DR, Lobl TJ, Seftor EA, et al. Use of the membrane invasion culture system (MICS) as a screen for anti-invasive agents. Int J Cancer 1989;43:449–457. [PubMed: 2925275]
29. Braun RD, Abbas A, Bukhari SO, Wilson W. Hemodynamic parameters in blood vessels in choroidal melanoma xenografts and rat choroid. Invest Ophthalmol Vis Sci 2002;43:3045–3052. [PubMed: 12202528]
30. Gamel JW, McLean I, Greenberg RA, et al. Objective assessment of the malignant potential of intraocular melanomas with standard microslides stained with hematoxylin-eosin. Hum Pathol 1985;16:689–692. [PubMed: 2408986]
31. Folberg R, Maniotis AJ. Vasculogenic mimicry. APMIS 2004;112:508–525. [PubMed: 15563313]
32. Rummelt V, Mehaffey MG, Campbell RJ, et al. Microcirculation architecture of metastases from primary ciliary body and choroidal melanomas. Am J Ophthalmol 1998;126:303–305. [PubMed: 9727526]
33. Clarijs R, Otte-Holler I, Ruiter DJ, de Waal RM. Presence of a fluid-conducting meshwork in xenografted cutaneous and primary human uveal melanoma. Invest Ophthalmol Vis Sci 2002;43:912–918. [PubMed: 11923228]
34. Lin AY, Maniotis AJ, Valyi-Nagy K, et al. Distinguishing fibrovascular septa from vasculogenic mimicry patterns. Arch Pathol Lab Med 2005;129:884–892. [PubMed: 15974811]
35. Chen X, Ai Z, Rasmussen M, et al. Three-dimensional reconstruction of extravascular matrix patterns and blood vessels in human uveal melanoma tissue: techniques and preliminary findings. Invest Ophthalmol Vis Sci 2003;44:2834–2840. [PubMed: 12824220]
36. Ai ZM, Chen X, Rasmussen M, Folberg R. Reconstruction and exploration of three-dimensional confocal microscopy data in an immersive virtual environment. Comput Med Imaging Graph 2005;29:313–318. [PubMed: 15893451]
37. Bajcsy P, Lee SC, Lin A, Folberg R. Three-dimensional volume reconstruction of extracellular matrix proteins in uveal melanoma from fluorescent confocal laser scanning microscope images. J Microsc 2006;221:30–45. [PubMed: 16438687]
38. Chen X, Maniotis AJ, Majumdar D, Pe'er J, Folberg R. Uveal melanoma cell staining for CD34 and assessment of tumor vascularity. Invest Ophthalmol Visual Sci 2002;43:2533–2539. [PubMed: 12147581]
39. Toivonen P, Makitie T, Kivela T. Microvessels and macrophages in choroidal and ciliary body melanoma Uveal melanoma: a model for exploring. Fundamental Cancer Biol 2004;177:189–2004.

40. Lin AY, Ai Z, Lee SC, et al. Comparing vasculogenic mimicry with endothelial cell lined vessels: techniques for 3D reconstruction and quantitative analysis of tissue components from archival paraffin blocks. Appl Immunohistochem Mol Morphol 2007;15:113–119. [PubMed: 17536318]
41. McDonald DM, Munn L, Jain RK. Vasculogenic mimicry: how convincing, how novel, and how significant? Am J Pathol 2000;156:383–388. [PubMed: 10666365]
42. McLean IW, Foster WD, Zimmerman LE, Martin DG. Inferred natural history of uveal melanomas. Invest Ophthalmol Vis Sci 1980;19:760–770. [PubMed: 7390722]
43. Kujala E, Makitie T, Kivela T. Very long-term prognosis of patients with malignant uveal melanoma. Invest Ophthalmol Vis Sci 2003;44:4651–4659. [PubMed: 14578381]
44. Foss AJE, Alexander RA, Hungerford JL, Harris AL, Cree IA, Lightman S. Re-assessment of the PAS patterns in uveal melanoma. Br J Ophthalmol 1997;81:240–246. [PubMed: 9135390]
45. Ruiter D, Bogenrieder T, Elder D, Herlyn M. Melanoma-stroma interactions: structural and functional aspects. Lancet Oncol 2002;3:35–43. [PubMed: 11905603]
46. Haaparanta T, Uitto J, Ruoslahti E, Engvall E. Molecular cloning of the cDNA encoding human laminin A chain. Matrix 1991;11:151–160. [PubMed: 1714537]
47. Kaiserman I, Amer R, Pe'er J. Liver function tests in metastatic uveal melanoma. Am J Ophthalmol 2004;137:236–243. [PubMed: 14962411]
48. Donoso LA, Shields JA, Augsburger JJ, Orth DH, Johnson P. Metastatic uveal melanoma: diffuse hepatic metastasis in a patient with concurrent normal serum enzyme levels and liver scan. Arch Ophthalmol 1985;103:758. [PubMed: 2860887]
49. Hicks C, Foss AJ, Hungerford JL. Predictive power of screening tests for metastasis in uveal melanoma. Eye 1998;12:945–948. [PubMed: 10325992]
50. Rivoire M, Kodjikian L, Baldo S, Kaemmerlen P, Negrier S, Grange JD. Treatment of liver metastases from uveal melanoma. Ann Surg Oncol 2005;12:422–428. [PubMed: 15886904]
51. Kulesa PM, Kasemeier-Kulesa JC, Teddy JM, et al. Reprogramming metastatic melanoma cells to assume a neural crest cell-like phenotype in an embryonic microenvironment. Proc Natl Acad Sci USA 2006;103:3752–3757. [PubMed: 16505384]
52. Folberg R, Arbieva Z, Moses J, et al. Tumor cell plasticity in uveal melanoma: microenvironment directed dampening of the invasive and metastatic genotype and phenotype accompanies the generation of vasculogenic mimicry patterns. Am J Pathol 2006;169:1376–1389. [PubMed: 17003493]

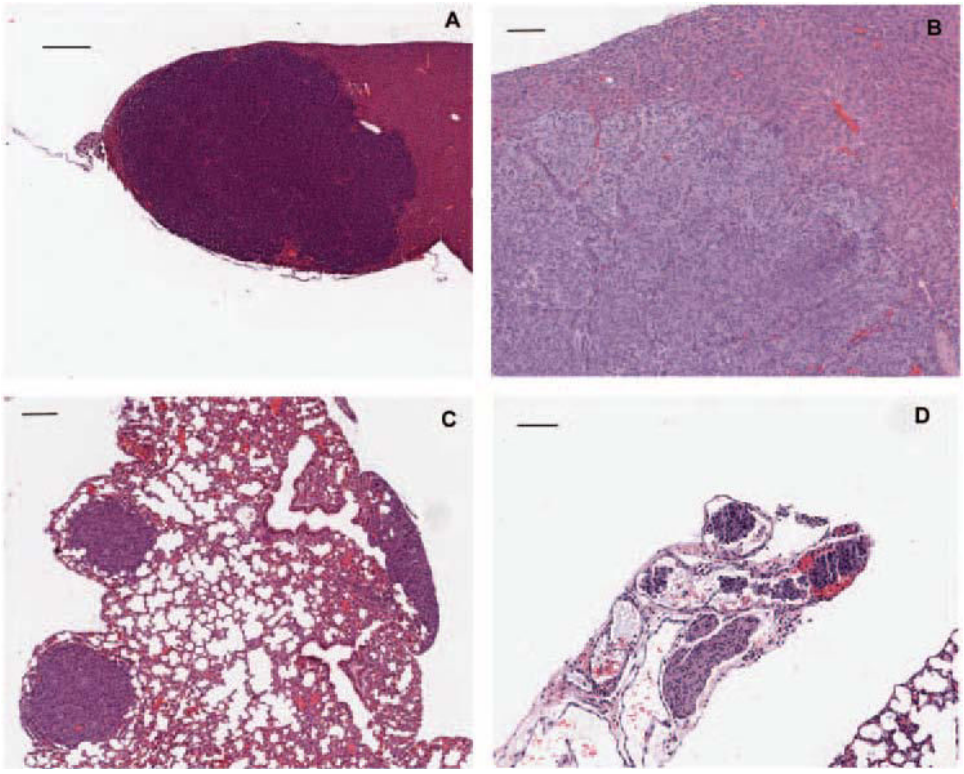

Figure 1.

Representative histologic sections of mouse liver at various times after injection with human uveal melanoma cell lines. (**A**) OCM1a cells formed a nodule in the mouse liver at 2 weeks after injection. (**B**) MUM2B cells in the mouse liver at 4 weeks after injection. (**C**) M619 cells formed secondary metastases to the lung 4 weeks after injection into the liver. (**D**) Tumor emboli were identified in hilar tissues adjacent to the lung (*bottom right*) from MUM2B cells 4 weeks after injection into the mouse liver. Bars: (**A**) 400 μm; (**B**, **D**) 100 μm; (**C**) 150 μm.

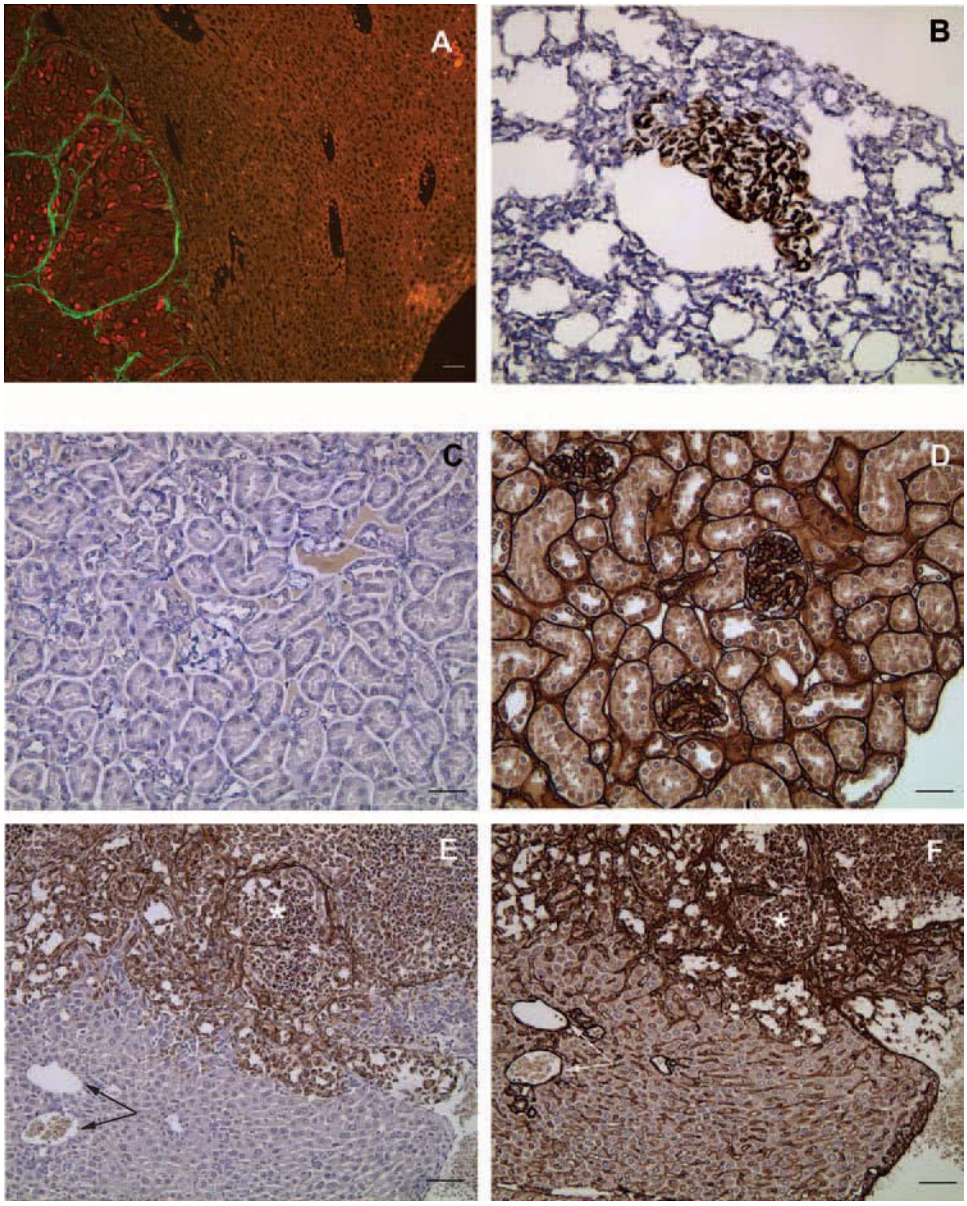

Figure 2.

Vasculogenic mimicry demonstrated in deposits of uveal melanoma in the SCID mouse liver. (**A**) Deposit of OCM1a in the mouse liver 6 weeks after injection. The tissue section has been labeled with an antibody to S100 protein (*red*) and to human laminin (*green*). Note the back-to-back loops of laminin within the tumor to the *left*. Blood vessels in the mouse liver do not label with human anti-laminin. (**B**) MUM2B cells metastatic to the mouse lung 4 weeks after implantation in the liver. The section is stained with antibody to human laminin and the reaction developed with diaminobenzidine (DAB). MUM2B cells are known to be amelanotic. Note the development of small laminin-positive loops within this very small secondary metastatic deposit. (**C**) Mouse kidney stained with antibody to human laminin. Neither the glomeruli nor the tubular basement membranes, both rich in laminin, stained with this antibody. (**D**) This section, stained with polyclonal antibody that cross-reacts with both human and mouse laminin, was taken adjacent to the section in (**C**). Note the staining of the mouse glomerular mesangium and tubular epithelium with this preparation developed with DAB. (**E**) Mouse liver into which

MUM2B cells were implanted 4 weeks before euthanatization. The tumor cells in the top half of the field were stained with an antibody to human laminin and developed with DAB. An *asterisk* is placed in the center of laminin-positive tumor cells surrounded by a laminin-positive loop. Note that blood vessels within the mouse liver did not stain with this antibody to human laminin (*arrows*). (**F**) This section, adjacent to (**E**), was stained with a polyclonal antibody that cross-reacts with both human and mouse laminin. Note that the tumor cells stained for laminin, loops were identified (note the *asterisk* in tumor cells surrounded by a loop), but in contrast to (**E**), the basement membranes of hepatic vessels stained positive with this antibody (*arrows*). Bars: (**A**–**D**) 100 μm; (**E**, **F**) 50 μm.

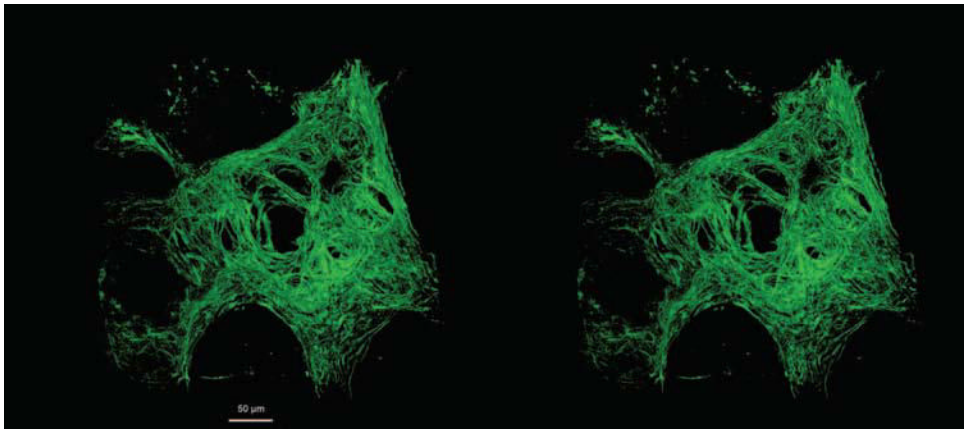

Figure 3.
Stereopair of a 3D reconstruction of a nodule of OCM1a cells 6 weeks after implantation. Sections used to develop this reconstruction were stained with antibody to human laminin (*green*). This preparation was also counterstained with antibody to S100 protein and developed with a *red* chromogen (as in Fig. 2A), but to reduce visual confusion, the red channel is not illustrated in this figure. Please also refer to Movie 1, http://www.iovs.org/cgi/content/full/48/7/2967/DC1, an animated GIF file of this reconstruction that clearly establishes the laminin-positive loops in 2D histologic sections (Fig. 2) and here represent the outlines of laminin-positive envelopes that are cylindrical.

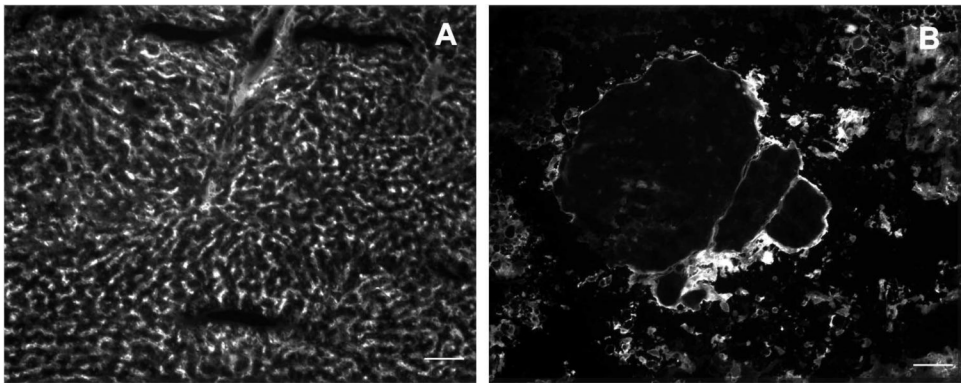

Figure 4.

Mouse liver containing OCM1a cells 6 weeks after implantation. This mouse was perfused with fluorescent BSA before euthanatization. (**A**) Fluorescence micrograph of this mouse's liver uninvolved in tumor. Note the presence of the fluorescent BSA filling the pattern of normal hepatic sinusoids. (**B**) Fluorescence micrograph taken from the same liver illustrated in (**A**), but illustrating the perfusion pattern in the tumor nodule formed by OCM1a cells. Note the presence of back-to-back loops in this 4-μm-thick section. Bar, 50 μm.

Table 1

Time Course of Melanoma Cells Implanted in the Mouse Liver

[[|]]	[[|]]	[[OCM1a|]]	[[M619|]]	[[MUM2B|]]
2 Weeks (*n* = 15)	[[Liver|]]	[[8|]]	[[10|]]	[[9|]]
[[|]]	[[Abdomen|]]	[[0|]]	[[0|]]	[[4|]]
[[|]]	[[Lung|]]	[[0|]]	[[0|]]	[[0|]]
4 Weeks (*n* = 15)	[[Liver|]]	[[9|]]	[[15|]]	[[15|]]
[[|]]	[[Abdomen|]]	[[0|]]	[[11|]]	[[14|]]
[[|]]	[[Lung|]]	[[0|]]	[[1|]]	[[8|]]
6 Weeks (*n* = 6)	[[Liver|]]	[[6|]]	[[|]]	[[|]]
[[|]]	[[Abdomen|]]	[[5|]]	[[|]]	[[|]]
[[|]]	[[Lung|]]	[[0|]]	[[|]]	[[|]]
7 Weeks (*n* = 2)	[[Liver|]]	[[2|]]	[[|]]	[[|]]
[[|]]	[[Abdomen|]]	[[2|]]	[[|]]	[[|]]
[[|]]	[[Lung|]]	[[1|]]	[[|]]	[[|]]
8 Weeks (*n* = 7)	[[Liver|]]	[[7|]]	[[|]]	[[|]]
[[|]]	[[Abdomen|]]	[[5|]] *	[[|]]	[[|]]
[[|]]	[[Lung|]]	[[5|]] *	[[|]]	[[|]]

Experiments were not extended beyond 4 weeks for cell lines M619 and MUM 2B.

* One animal with abdominal involvement had no pulmonary metastases, and one animal with pulmonary metastases has no abdominal involvement.

Table 2

Sizes of Uveal Melanoma Nodules in the Mouse Liver by Cell Line and Time

[[|]]	OCM1a					M619					MUM2B				
[[Time in Weeks|]]	**[[Mean|]]**	**[[SD|]]**	***n***	**[[Min|]]**	**[[Max|]]**	**[[Mean|]]**	**[[SD|]]**	***n***	**[[Min|]]**	**[[Max|]]**	**[[Mean|]]**	**[[SD|]]**	***n***	**[[Min|]]**	**[[Max|]]**
[[2|]]	[[0.53|]]	[[0.39|]]	[[7|]]	[[0.23|]]	[[1.3|]]	[[1|]]	[[1.13|]]	[[10|]]	[[0.27|]]	[[4|]]	[[1.46|]]	[[0.98|]]	[[9|]]	[[0.42|]]	[[3.1|]]
[[4|]]	[[1.81|]]	[[2.44|]]	[[10|]]	[[0.2|]]	[[8.5|]]	[[4.12|]]	[[1.52|]]	[[15|]]	[[1.35|]]	[[7|]]	[[3.11|]]	[[1.92|]]	[[15|]]	[[0.9|]]	[[6.5|]]
[[6|]]	[[4.63|]]	[[1.81|]]	[[6|]]	[[1.8|]]	[[7|]]	[[|]]	[[|]]	[[|]]	[[|]]	[[|]]	[[|]]	[[|]]	[[|]]	[[|]]	[[|]]
[[7|]]	[[4.93|]]	[[4.35|]]	[[2|]]	[[1.85|]]	[[8|]]	[[|]]	[[|]]	[[|]]	[[|]]	[[|]]	[[|]]	[[|]]	[[|]]	[[|]]	[[|]]
[[8|]]	[[6.54|]]	[[4.48|]]	[[7|]]	[[1.2|]]	[[15|]]	[[|]]	[[|]]	[[|]]	[[|]]	[[|]]	[[|]]	[[|]]	[[|]]	[[|]]	[[|]]

Data are in millimeters. Statistical comparisons (Kruskal-Wallis test): OCM1a: 2 weeks vs. 8 weeks: $P = 0.026$ ($df = 1$, $\chi^2 = 9.0362$); M619: 2 weeks vs. 4 weeks: $P = 0.0002$ ($df = 1$, $\chi^2 = 13.941$); MUM2B: 2 weeks vs. 4 weeks: $P = 0.0273$ ($df = 1$, $\chi^2 = 4.8718$).

Invest Ophthalmol Vis Sci. Author manuscript; available in PMC 2008 July 1.